Electronic Supplementary Information

Enantiomeric Fe(II)-incorporated organic-inorganic hybrid crystals for energy harvesting

Dan Lu, Yun-Hui Yu, Yong Yu, Yan-Ran Weng, Jia-Zi She, and Yong Ai*

Corresponding author: yong.ai@ncu.edu.cn

Experimental Section

Materials. *R*/*S*-3-quinuclidinol was purchased from Macklin and used as received. Iron chloride ($FeCl_2$) and hydrochloric acid (HCl) were sourced from Adamas, while methanol was obtained from Aladdin. Given the high sensitivity of Fe^{2+} to oxygen, all the experimental procedures were meticulously conducted under an inert atmosphere to avoid oxidation.

Single-crystal X-ray diffraction (XRD). The single-crystal X-ray diffraction (XRD) data were collected on a Rigaku Oxford diffractometer (Cu Kα, λ=1.54184). The SHELX program package on the Olex2 program was used to solve the structural data and perform structural refinement. CCDC 2392645-2392646 contains the supplementary crystallographic data for this paper. These data can be obtained free of charge via www.ccdc.cam.ac.uk/data_request/cif, by emailing data_request@ccdc.cam.ac.uk, or by contacting The Cambridge Crystallographic Data Centre, 12 Union Road, Cambridge CB2 1EZ, UK; fax: +44 1223 336033.

Powder X-ray diffraction (PXRD). The variable-temperature powder X-ray diffraction (PXRD) data were collected by using a Rigaku D/MAX 2000 PC X-ray diffraction system. Cu Kα radiation was employed with a 2θ range of 5-40° and a step size of 0.02°.

Thermogravimetric Analysis (TGA) Measurements, **Differential Scanning Calorimetry (DSC)**, and **Second Harmonic Generation (SHG)** and **Dielectric Measurements**. TGA from 300 to 900K was performed by using PerkinElmer TGA 8000. The DSC measurements were recorded on a NETZSCH DSC 200 F3 instrument. The crystalline samples were heated and cooled at a rate of 10 $K \cdot min^{-1}$ in an aluminum crucible under a nitrogen atmosphere. SHG measurements were performed by FLS 920, Edinburgh Instruments using an unexpanded laser beam with low divergence (pulsed Nd: YAG at a wavelength of 1064 nm). The laser is Vibrant 355 II, OPOTEK. The complex permittivity in the temperature range of 320-370 K was measured by using Tong hui TH2828A.

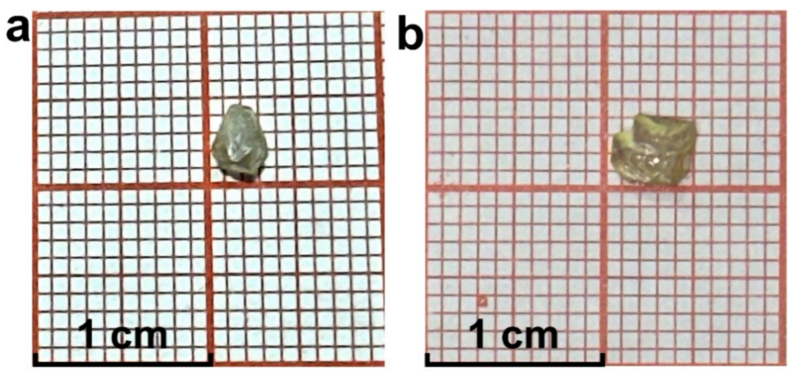

Figure S1. Photograph of the crystal of (a) $(R\text{-HQ})_2FeCl_4$ and (b) $(S\text{-HQ})_2FeCl_4$.

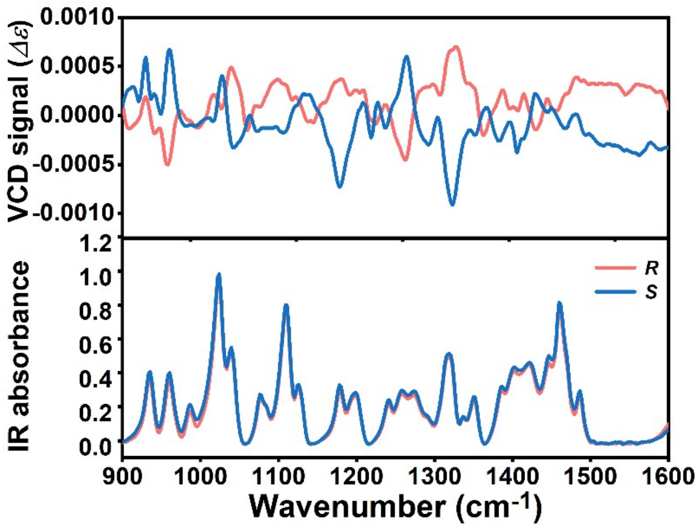

Figure S2. Experimentally measured VCD and IR spectra for (R/S-HQ)$_2$FeCl$_4$.

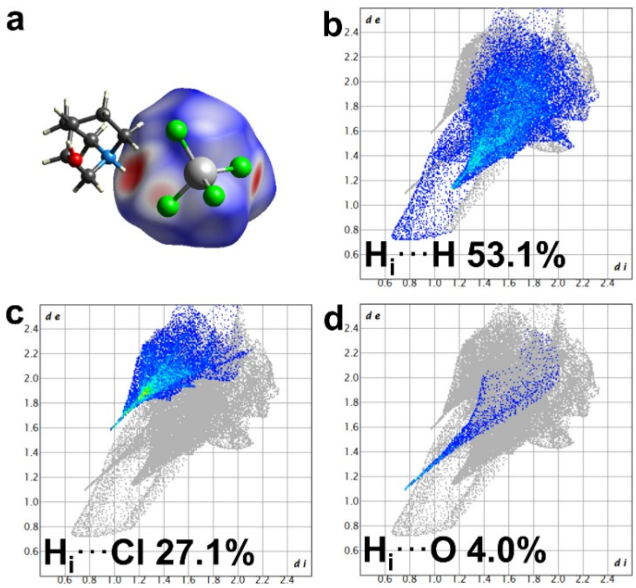

Figure S3. (a) Visualization map of the distribution of the interactions and the 2D fingerprint plots of (S-HQ)$_2$FeCl$_4$. And the 2D fingerprint plots of H_i−H (b), H_i−Cl (c), and H_i−O (d) of (S-HQ)$_2$FeCl$_4$.

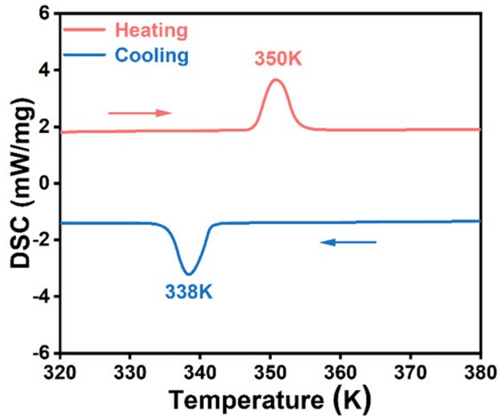

Figure S4. DSC curves of (S-HQ)$_2$FeCl$_4$ in a heating-cooling mode.

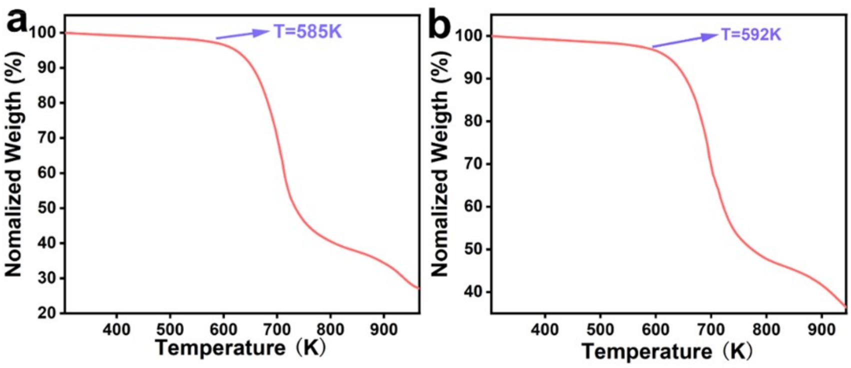

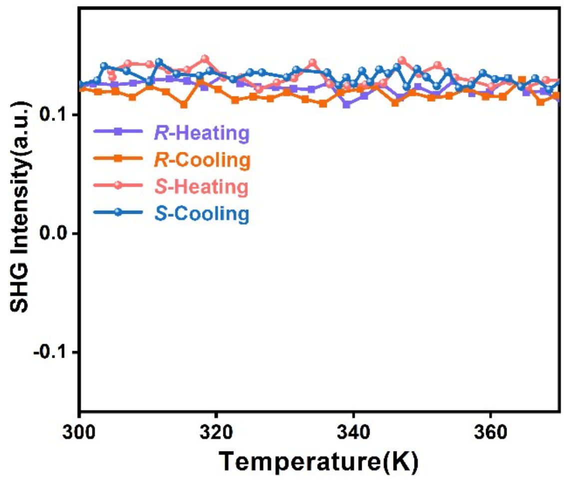

Figure S5. (a) TGA curves of (R-HQ)$_2$FeCl$_4$. (b) TGA curves of (S-HQ)$_2$FeCl$_4$.

Figure S6. (a) Temperature-dependent SHG responses of (R/S-HQ)$_2$FeCl$_4$.

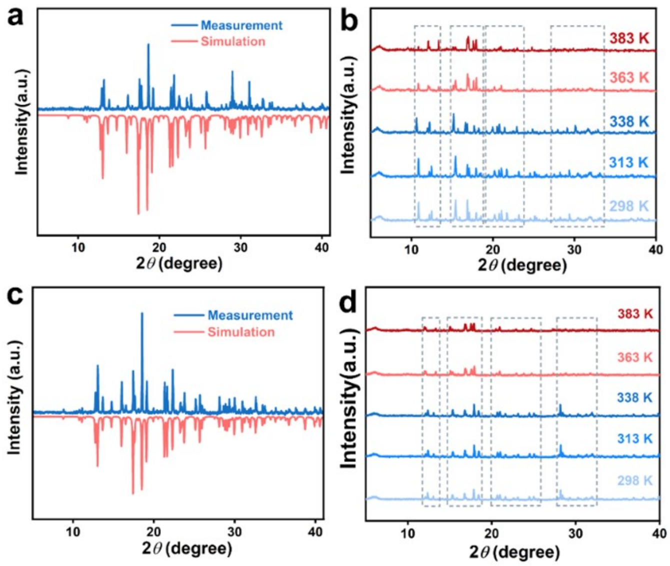

Figure S7. (a)The measured and simulated PXRD patterns of (*R*-HQ)$_2$FeCl$_4$. (b)The variable-temperature PXRD patterns of (*R*-HQ)$_2$FeCl$_4$. (c)The measured and simulated PXRD patterns of (*S*-HQ)$_2$FeCl$_4$. (d)The variable-temperature PXRD patterns of (*S*-HQ)$_2$FeCl$_4$.

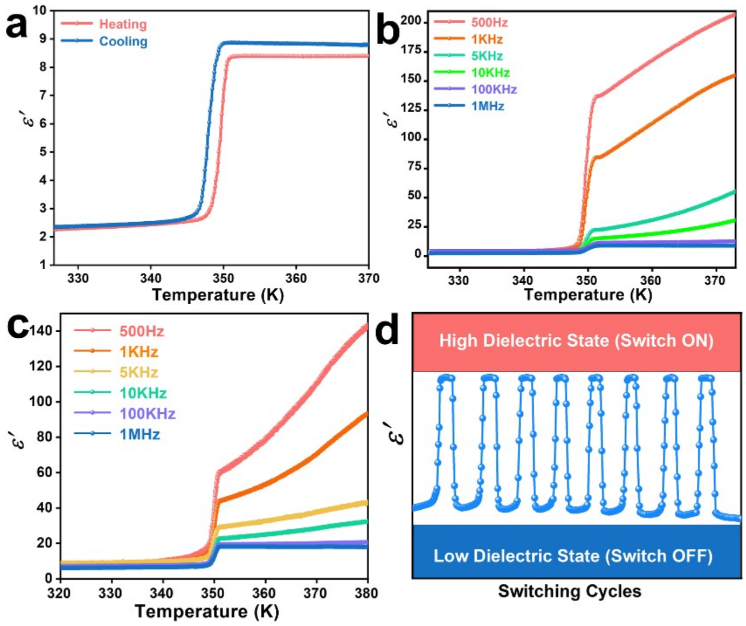

Figure S8. (a) The dielectric measurements of (*S*-HQ)$_2$FeCl$_4$. (b) Temperature-dependent dielectric constants of (*R*-HQ)$_2$FeCl$_4$ at different frequencies. (c) Temperature-dependent dielectric constants of (*S*-HQ)$_2$FeCl$_4$ at different frequencies. (d) The dielectric switch test of (*S*-HQ)$_2$FeCl$_4$.

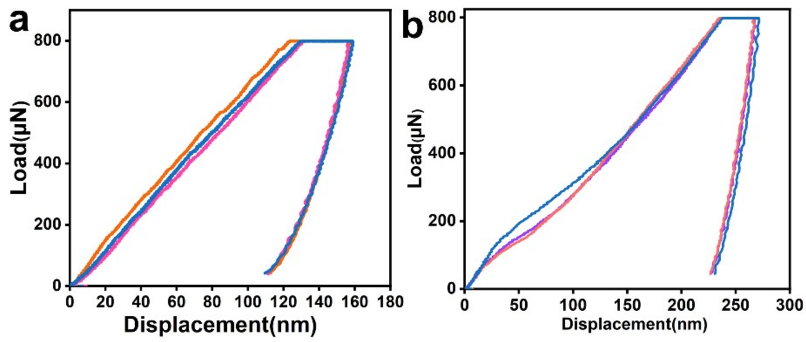

Figure S9. Load-displacement curves of the single crystal (a) (R-HQ)$_2$FeCl$_4$, (b) (S-HQ)$_2$FeCl$_4$ crystals were measured.

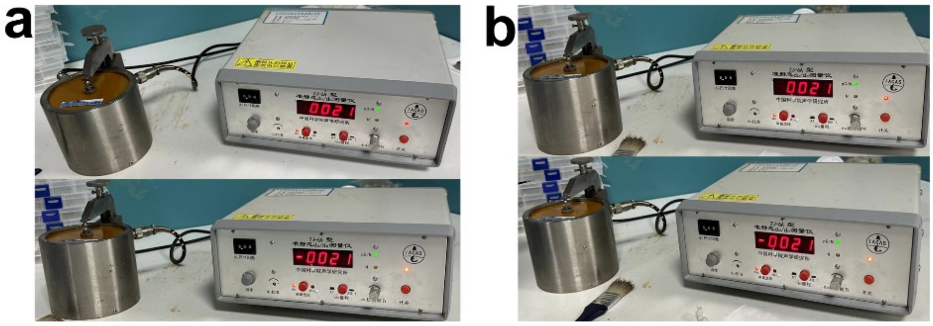

Figure S10. Measurements of d_{33} value of (a) (R-HQ)$_2$FeCl$_4$ and (c) (S-HQ)$_2$FeCl$_4$.

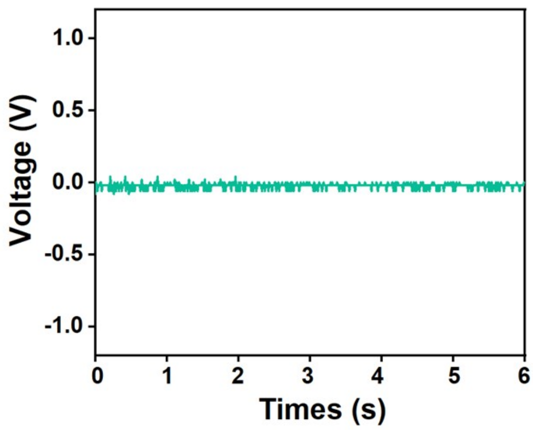

Figure S11. A blank device without piezoelectric crystals generated weak output voltages for the piezoelectric energy harvester.

Table S1. Crystal data and structure refinement for (R/S-HQ)$_2$FeCl$_4$ at 293 K.

Molecule	(R-HQ)$_2$FeCl$_4$	(S-HQ)$_2$FeCl$_4$
Temperature	293K	293K
Crystal system	Orthorhombic	Orthorhombic
Formula weight	452.02	452.02
Space group	$P2_12_12_1$	$P2_12_12_1$
a/ Å	12.9615(3)	9.6552(14)
b/ Å	9.5813(2)	13.0538(15)
c/ Å	15.9455(3)	16.078(2)
α/°	90	90
β/°	90	90
γ/°	90	90
Volume/ Å^3	1980.24(7)	2026.4(5)
Z	4	4
Radiation	$Cu\ K\alpha$(λ=1.54184)	$Cu\ K\alpha$(λ=1.54184)
ρcalc g/cm^3	1.516	1.482
F (000)	936.0	936.0
GOF	1.058	1.096
R_1[I > 2σ(I)]	0.0595	0.0525
wR_2[I > 2σ(I)]	0.1698	0.1683

Table S2. Hydrogen Bonds for (R-HQ)$_2$FeCl$_4$ at 293 K.

D	H	A	d(D-H)/Å	d(H-A)/Å	d(D-A)/Å	D-H-A/°
O1	H1	Cl1	0.65	2.41	2.959(9)	144
N1	H1A	O1	0.98	1.81	2.754(10)	161
N1	H1A	O3	0.98	1.88	2.833(17)	163
N2	H2	O2	0.98	1.85	2.800(9)	164
O2	H2A	Cl4	0.82	2.32	3.126(7)	166
C1	H1B	Cl2	0.97	2.80	3.540(7)	134
C13	H13A	Cl1	0.97	2.66	3.631(11)	177

Table S3. Hydrogen Bonds for (S-HQ)$_2$FeCl$_4$ at 293 K.

D	H	A	d(D-H)/Å	d(H-A)/Å	d(D-A)/Å	D-H-A/°
N1	H1	O1	0.98	1.84	2.7899	162
N1	H1	O1A	0.98	1.93	2.88615	163
O1A	H1AA	N1	0.82	2.47	2.88615	113
O1	H1B	N1	0.82	2.33	2.7899	116
O2	H2	Cl3	0.82	2.34	3.1405	165
N2	H2B	O2	0.98	1.89	2.8469	164
C4	H4B	Cl4	0.97	2.82	3.5666	134
C10	H10B	Cl2	0.97	2.69	3.65911	177

Table S4. The comparison of piezoelectric coefficients d_{33} of different types of compounds.

Compound type		compound	d_{33}(pC/N)
Ionic crystals	Inorganic oxides	BTO[001](poling)[1]	110
		$LiNbO_3$[2]	11
		ZnO[3]	3
	hybrid compounds	$[AH][ReO_4]$[4]	90
		TGS[5]	22
		This work	21
		$[Me_3NOH]_2[KFe(CN)_6]$[6]	20
		$HQReO_4$[7]	19
		[N-methylpyrrolidinium]$_3Sb_2Br_9$[8]	12
		(R-3-hydroxypyrrolidinium)$_2RbBiBr_6$[9]	11
		$[(C_2H_5)_4N][FeBrCl_3]$[10]	7.7
		Rochelle Salt[11]	7
		$(C_4H_9NH_3)_2PbCl_4$[12]	5.5
		[3-pyrrolinium]$MnCl_3$[13]	4
Molecular crystals	single-component compounds	5-lodo-2-adamantanone[14]	5
		Croconic acid[15]	5
		Lysozyme[16]	6.5
		DL-alanine[17]	4.8
		Small intestinal submucosa[18]	4.1
	polymers	PVDF[19]	28
		ploy(L-lactic acid)[20]	10.2
		Nylon-11[21]	2

References:

1. Wang, Z.; Cheng, J.; Hu, R.; Yuan, X.; Yu, Z.; Xu, X.; Wang, F.; Dong, J.; Gong, R.; Dong, S. An approach combining additive manufacturing and dielectrophoresis for 3D-structured flexible lead-free piezoelectric composites for electromechanical energy conversion. *J. Mater. Chem. A*, 2021, **9**, 26767-26776.
2. R. S. Weis, T. K. Gaylord, Lithium niobate: Summary of physical properties and crystal structure. *Appl. Phys*., 1985, **37**, 191-203.
3. D. A. Scrymgeour, T. L. Sounart, N. C. Simmons, J. W. P. Hsu, Polarity and piezoelectric response of solution grown zinc oxide nanocrystals on silver. *J. Appl. Phys*, 2007, **101**, 014316.
4. J. Harada, Y. Kawamura, Y. Takahashi, Y. Uemura, T. Hasegawa, H. Taniguchi and K. Maruyama, Plastic/Ferroelectric Crystals with Easily Switchable Polarization: Low-Voltage Operation, Unprecedentedly High Pyroelectric Performance, and Large Piezoelectric Effect in Polycrystalline Forms, *J. Am. Chem. Soc*., 2019, **141**, 9349-9357.
5. R. G. Xiong, The temperature-dependent domains, SHG effect and piezoelectric coefficient of TGS, *Chin. Chem. Lett*., 2013, **24**, 681-6844.
6. W. J. Xu, P. F. Li, Y.Y. Tang, W. X. Zhang, R. G. Xiong, X.-M. Chen, A molecular perovskite with switchable coordination bonds for high-temperature multiaxial ferroelectrics. *J. Am. Chem. Soc*., 2017, **139**, 6369-6375.
7. E. D. Sødahl, J. Walker and K. Berland, Piezoelectric Response of Plastic Ionic Molecular Crystals: Role of Molecular Rotation, *Cry. Growth Des*., 2023, **23**, 729-740.
8. Z. Sun, A. Zeb, S. Liu, C. Ji, T. Khan, L. Li, M. Hong, J. Luo, Exploring a lead-free semiconducting hybrid ferroelectric with a zero-dimensional perovskite-like structure. *Angew. Chem. Int. Ed*.,2016, **55**, 11854-11858.
9. L. He, P. P. Shi, L. Zhou, Z. B. Liu, W. Zhang, Q. Ye, Coexisting ferroelectric and ferroelastic orders in rare 3D homochiral hybrid bimetal halides. *Chem. Mater*., 2021, **33**, 6233-6239.
10. J. Walker, E. D. Sødahl, S. Scherrer, K. Marshall, D. Chernyshov, K. Berland and T. Rojac, Electromechanical properties of uniaxial polar ionic plastic crystal $[(C_2H_5)_4N][FeBrCl_3]$, *J. Phys. Energy*., 2024, **6**, 025026.
11. E. Lemaire, R. Moser, C. J. Borsa, D. Briand, Green paper-based piezoelectronics for sensors and actuators. Sens. *Actuators A Phys*., 2016, **244**, 285-2919.
12. D. Li, X. M. Zhao, H. X. Zhao, X. W. Dong, L. S. Long, L. S. Zheng, Construction of magnetoelectric composites with a large room-temperature magnetoelectric response through molecular-ionic ferroelectrics. *Adv. Mater*.,2018, **30**, e18037169.
13. H. Y. Ye, Q. Zhou, X. Niu, W. Q. Liao, D. W. Fu, Y. Zhang, Y. M. You, J. Wang,

Z. N. Chen, R. G. Xiong, High-temperature ferroelectricity and photoluminescence in a hybrid organic-inorganic compound: (3-Pyrrolinium)$MnCl_3$. *J. Am. Chem. Soc.*, 2015, **137**, 13148-131549.

14. L. Xu, Y. Zhang, H. H. Jiang, N. Zhang, R. G. Xiong, H. Y. Zhang, Solvent selective effect occurs in iodinated adamantanone ferroelectrics. *Adv. Sci.*, 2022, **9**, e2201702.
15. S. Horiuchi, Y. Tokunaga, G. Giovannetti, S. Picozzi, H. Itoh, R. Shimano, R. Kumai, Y. Tokura, Above-room-temperature ferroelectricity in a single-component molecular crystal. *Nature.*, 2022, **463**, 789-7922.
16. A. Stapleton, M. R. Noor, J. Sweeney, V. Casey, A. L. Kholkin, C. Silien, A. A. Gandhi, T. Soulimane, S. A. M. Tofail, The direct piezoelectric effect in the globular protein lysozyme. Appl. Phys. Lett., 2017, **111**, 142902.
17. S. Guerin, J. O'Donnell, E. U. Haq, C. McKeown, C. Silien, F. M. F. Rhen, T. Soulimane, S. A. M. Tofail, D. Thompson, Racemic amino acid piezoelectric transducer. *Phys. Rev. Lett.*, 2019, **122**, 047701.
18. Z. Zhang, S. Liu, Q. Pan, Y. Hong, Y. Shan, Z. Peng, X. Xu, B. Liu, Y. Chai, Z. Yang, Vander Waals exfoliation processed biopiezoelectric submucosa ultrathin films. *Adv. Mater.*, 2022, **34**, e2200864.
19. W. Lian, M. Zhang, J. Wang, C. Wu, K. Lamnawar, A. Maazouz, B. Lu, B. Dong, C. Liu, Interface-engineered composite nanofibers for boosting piezoelectric outputs of polymeric nanogenerators. *Mater. Lett.*, 2023, **349**, 134860.
20. X. Du, C. Zhao, J. Zhang, K. Ren, Study of field-induced chain conformation transformation in poly(*L*-lactic acid) based piezoelectric film by infrared spectroscopy. *J. Appl. Phys.*, 2016, **120**, 164101.
21. E. K. Akdogan, M. Allahverdi, A. Safari, Piezoelectric composites for sensor and actuator applications. *Trans. Ultrason. Ferroelectr. Freq. Control.*, 2005, **52**, 746-775.